Molecular Recognition in Cyclodextrin Complexes of Amino Acid Derivatives: The Effects of Kinetic Energy on the Molecular Recognition of a Pseudopeptide in a Nonconstraining Host Environment as Revealed by a Temperature-Dependent Crystallographic Study

Joanna L. Clark, Jessica Peinado, John J. Stezowski,* Robert L. Vold,† Yuanyuan Huang, and Gina L. Hoatson

Department of Chemistry, University of Nebraska-Lincoln, Lincoln, Nebraska 68588-0304, and Departments of Applied Science and Physics, College of William and Mary, P.O. Box 8795, Williamsburg, Virginia 23187-8795

Received: August 13, 2006; In Final Form: October 6, 2006

The crystal structure of a triclinic 2:2 inclusion complex of β-cyclodextrin with *N*-acetyl-L-phenylalanine methyl ester has been determined at several temperatures between 298 and 20 K to further study molecular recognition using solid-state supramolecular β-cyclodextrin complexes. The study reveals kinetic energy dependent changes in guest molecule conformations, orientations, and positions in the binding pocket presented by the crystal lattice. Accompanying these changes are observable differences in guest−guest interactions and hydrogen-bonding interactions in the binding pocket that involve guest molecules, water of hydration molecules, and β-cyclodextrin molecules. On the basis of the differences observed in the crystal structures, we present a solid-state example of a system that displays the properties of both classical and quantum chemical models. At higher temperatures, the structure conforms to a classical mechanical model with dynamic disorder. At lower temperatures, the observations conform to examples in which there is static disorder representative of models in which quantum states differing in conformation, position, and orientation of components in the crystal structure are occupied. Ab initio theoretical calculations on the different guest molecule conformations have been carried out. Superpositions of theoretical electrostatic surface potential diagrams on the observed molecular positions in the complexes provide confidence that the deconvolution of the guest molecule disorder is acceptable. Temperature-dependent solid-state magic angle spinning deuteron NMR measurements provide evidence for large-amplitude, diffusive motion on a microsecond time scale in the complex.

Introduction

Molecular recognition is an important phenomenon that occurs due to a combination of noncovalent intermolecular interactions.[1,2] One of the primary roles in molecular recognition is played by geometric complementarity, or spatial fit.[3,4] Other important interactions include hydrogen-bonding, hydrophobic, and Coulombic interactions.[5] Molecular recognition is important in many life processes involving large macromolecules and also plays a critical role in the design of solid-state materials with novel properties.

Crystallographic studies relevant to molecular recognition are typically based on structure determinations for macromolecular systems in which the resolution is relatively low, or on small-molecule studies of neat systems in which interactions are confined to molecules of the same kind or, at best, between the small molecules and a very small number of molecules of solvation.

Studies from this laboratory have examined molecular interactions in single crystals of hydrated 2:2 supramolecular β-cyclodextrin (β-CD) complexes with *N*-acetyl-L-phenylalanine derivatives in nearly isomorphous structures and found that the crystal lattice provides an interesting binding pocket model for the systematic study of molecular recognition.[6,7] The model is based on a commonly observed β-CD dimer-packing motif, the triclinic intermediate (IM) type. The binding pocket model involves both a nonspecific hydrophobic pocket (the interior of a β-CD hydrogen-bonded dimer) in one layer of the crystal structure and its two surrounding hydrophilic interface regions, composed of primary hydroxyls of neighboring β-CD dimers and waters of hydration. Appropriate β-CD molecules in the packing motif provide a defined array of primary hydroxyl groups that serve as hydrogen-bond donor/acceptor moieties analogous to those of a macromolecular receptor. They interact with *N*-acetyl-L-phenylalanine derivative substrate molecules either directly or via bridging water molecules to provide different experimental examples of molecular recognition that are determined by the structure of the substrate molecules and their intermolecular interactions. The effects of minor changes in backbone structure[2] and of side-chain structure[3] have been reported. This report examines the effects of an additional important variable, kinetic energy, on the interactions between the binding pocket and a selected substrate molecule, *N*-acetyl-L-phenylalanine methyl ester, a depsipeptide analogue.

The kinetic energy content of a crystal can be controlled, though not easily quantified, by adjusting the temperature of the crystal. We have determined the crystal structure of the hydrated 2:2 complex of β-CD with *N*-acetyl-L-phenylalanine methyl ester (*N*-Ac-L-FOMe) at a number of temperatures between room temperature (∼298 K) and 20 K and have measured 17.6 T solid-state magic angle deuteron NMR spectra at 300, 270, and 230 K. The *N*-acetyl-L-phenylalanine methyl ester substrate molecules were disordered in the crystal; the

* Corresponding author. E-mail: jstezowski1@unl.edu.
† Departments of Applied Science and Physics, College of William and Mary.

10.1021/jp0652244 CCC: $33.50
Published on Web 12/21/2006

disorder was deconvoluted to reveal remarkable changes in orientation, position, and conformation of the substrate molecules. The changes represent the operation of different mechanisms of molecular recognition as a function of the kinetic energy of the crystal.

The presence of disorder is interpreted as an indication that the modes of molecular recognition observed at each temperature are of similar potential energy. The change in apparent nature of the disorder from dynamic at higher temperatures to static at lower temperatures provides illustrations of a transition in the system from a classical mechanical model to a quantum mechanical one. Differences in occupancy factors of the guests in the statically disordered structures may reflect subtle differences in quantum energy levels. Ab initio theoretical calculations were used to assess the differences in conformational energy of individual guest molecules.

Experimental Section

Crystal Structure Determinations. Single crystals of the 2:2 *N*-Ac-L-FOMe/β-CD complex were grown by slow evaporation from an aqueous solution. The complex crystallizes in the triclinic space group *P*1 with one example of the 2:2 complex and ~25 water molecules per unit cell. No evidence for a change in space group as a function of crystal temperature was found. Crystal properties are characterized as a function of temperature in Table 1. Data, which for practical reasons were collected from four different crystals, were corrected for Lorentz and polarization effects, but not for absorption ($\mu = 0.0123$ to 0.125 mm^{-1}). Complete sets of diffraction data were collected from two different crystals at room temperature in order to check the structural integrity of crystals grown at different times and in different laboratories. One data set was collected several years ago,[8] from a crystal grown in Stuttgart, Germany, with a Siemens P3 four-circle diffractometer on a sealed tube X-ray generator; another data set was collected from a freshly grown crystal in Lincoln, NE, using a Bruker AXS rotating anode generator coupled with a MARResearch 18 cm imaging plate area detector. The two data sets yielded identical crystal structure models within experimental error; the results from the four-circle diffractometer are used here. Data sets collected at 260 and 265 K were of lower quality than those at other temperatures, which may reflect the fact that the crystal had undergone numerous temperature changes before these particular data sets were collected. Because crystals of hydrated cyclodextrin complexes typically decompose due to loss of solvent on exposure to air, all crystals were mounted in glass capillaries with mother liquor to maintain constant hydration.

Initial crystal structure models were derived from the isomorphous thermodynamically stable phase of the *n*-propanol complex reported earlier[9,10] and subsequently with one of the complexes in this series. The starting model in each case consisted of the carbon and oxygen atoms (excluding O6-atoms) of the β-CD dimer. SHELXL-97 was used for model development and refinement. Missing cyclodextrin oxygen atoms were located in difference electron density maps as were water oxygen atoms. Idealized models for the *N*-Ac-L-FOMe were fit to subsequent difference electron density maps (visualized using InsightII, version 98.0[11]) by adjustment of appropriate torsion angles accompanied with rotation and translation operations. Appropriate hydrogen atoms were typically added to the models using standard geometrical considerations and refined with a riding model. Carbon and oxygen atoms of the β-CD molecules were refined with anisotropic atomic displacement parameters as were the oxygen atoms of well-ordered water molecules. Oxygen atoms of less-well-ordered water molecules were refined with isotropic atomic displacement parameters. Guest molecules with high populations were generally refined as rigid bodies with restrained individual atomic displacement parameters. Guest molecules with lower populations (typically less than 25%) were refined as rigid bodies with an overall atomic displacement parameter. The refinements are characterized in Table 2. Intermolecular interactions were analyzed with the aid of the Parst97 program.[12]

Deuteron Magic Angle Spinning. For NMR experiments, *N*-acetyl-L-phenylalanine methyl ester (α,β,β,2,3,4,5,6-d_8) was prepared in Lincoln, NE, according to procedures described elsewhere, starting from deuterated L-phenylalanine-d_8 (Sigma Aldrich). Deuteron magic angle spinning (MAS) spectra of the 2:2 complex of β-CD with the labeled *N*-Ac-L-FOMe) were obtained at the College of William and Mary using a Bruker WB 750 NMR spectrometer operating at 17.6 T (115.1 MHz for ^{2}H). The spin rate was 15 kHz, the 90° pulse width was 1.4 μs, and 8 K scans with 8 or 16 K complex points were acquired. At all temperatures, a 0.5 s recycle delay was adequate for full recovery between scans. The temperature was controlled to better than $\pm$0.1 K using the Bruker temperature controller; the reported values have been corrected for frictional heating based on calibration against lead nitrate.

Theoretical Calculations. Ab initio calculations were carried out using SPARTAN '02 Windows employing hybridized DFT-Hartree−Fock basis sets at the B3LYP-6-31G** level. The molecular conformations observed in the crystal structures were used as starting models for each calculation. Constraints were applied to five torsion angles: the conventional peptide torsion angles: ψ, φ, χ_1, χ_2, and the torsion angle defining the ester methyl group position. The program was also used to calculate molecular dipoles and electrostatatic potential surfaces.

Results and Discussion

The complex crystallizes with the intermediate (Im) (or cage-type) packing motif for hydrated head-to-head dimeric β-cyclodextrin complexes.[13] Two pseudopeptide guest molecules are included in the hydrogen-bonded β-CD dimer (one per monomer). In our previous reports on amino acid derivatives in β-CD, we defined three domains in the intermediate-packed crystals: (a) a hydrogen-bonded β-CD dimer that presents an extended hydrophobic toroidal region for guest molecules, (b) a hydrophilic interdimer region where waters of hydration and neighboring primary hydroxyls are available for interaction with included guest molecules, and (c) a region between CD dimers where waters play primarily a space-filling role; that is, they are not close enough for guest molecule interactions. This report focuses on temperature-dependent changes that occur in the first two domains.

As the *N*-Ac-L-FOMe/β-CD crystal is cooled, the unit cell volume decreases systematically without thus far revealing evidence for a crystal symmetry related phase transition. Figure 1 illustrates the host and guest molecule structures at three temperatures (298, 220, and 20 K); the disordered guest molecules are presented with their respective difference electron densities. The disorder is deconvoluted in Figure 2, which illustrates the changes in conformation and position of the guest molecules as the kinetic energy of the crystals is reduced. The deconvoluted structures for the complexes are grouped by crystal temperature and are positioned to place similar conformations in columns in the figure. One set of complexes, the A2−B2 pairs, cannot pack sequentially in stacks in the crystal because of unfavorable contacts; they must be mixed with other combinations within a stack.

TABLE 1: Crystallographic Data Collection Details

T (K)	lattice parameters	intensity data	resolution	no. H_2O refined[d]	crystal size (mm)	*R*(int)
298(2)	$a = 18.129(2)$ Å $b = 15.411(2)$ Å $c = 15.585(2)$ Å $\alpha = 103.97(1)^\circ$ $\beta = 112.89(1)^\circ$ $\gamma = 98.79(1)^\circ$ $V = 3741.7$ Å^3	F-CD[a] no. raw data: no. unique data: 13217	0.84 Å	23.35	0.7 × 0.7 × 0.4	NA
270(1)	$a = 18.07(6)$ Å $b = 15.38(6)$ Å $c = 15.55(6)$ Å $\alpha = 104.07(6)^\circ$ $\beta = 113.02(6)^\circ$ $\gamma = 98.53(6)^\circ$ $V = 3712.8$ Å^3	AD[b] no. raw data: 32290 no. unique data: 14369	0.80 Å	23.75	0.5 × 0.4 × 0.2	0.041
265(1)	$a = 18.03(6)$ Å $b = 15.36(6)$ Å $c = 15.54(6)$ Å $\alpha = 103.83(6)^\circ$ $\beta = 113.06(6)^\circ$ $\gamma = 98.61(6)^\circ$ $V = 3693.7$ Å^3	AD[c] no. raw data: 22746 no. unique data: 11819	0.83 Å	20.75	0.6 × 0.5 × 0.2	0.022
260(1)	$a = 17.97(6)$ Å $b = 15.39(6)$ Å $c = 15.51(6)$ Å $\alpha = 103.18(6)^\circ$ $\beta = 113.23(6)^\circ$ $\gamma = 98.91(6)^\circ$ $V = 3670$ Å^3	AD[c] no. raw data: 21159 no. unique data: 11615	0.83 Å	22.40	0.6 × 0.5 × 0.2	0.023
220(2)	$a = 17.915(2)$ Å $b = 15.405(3)$ Å $c = 15.542(2)$ Å $\alpha = 103.04(1)^\circ$ $\beta = 113.35(1)^\circ$ $\gamma = 99.05(1)^\circ$ $V = 3687.6$ Å^3	F-CD[a] no. raw data: no. unique data: 12939	0.84 Å	26	0.7 × 0.7 × 0.4	NA
110(2)	$a = 17.896(2)$ Å $b = 15.389(3)$ Å $c = 15.519(2)$ Å $\alpha = 103.01(1)^\circ$ $\beta = 113.43(1)^\circ$ $\gamma = 99.07(1)^\circ$ $V = 3672.0$ Å^3	F-CD[a] no. raw data: no. unique data: 13217	0.84 Å	24.20	0.7 × 0.7 × 0.4	NA
20(1)	$a = 17.78(6)$ Å $b = 15.31(6)$ Å $c = 15.35(6)$ Å $\alpha = 102.76(6)^\circ$ $\beta = 113.31(6)^\circ$ $\gamma = 99.24(6)^\circ$ $V = 3596$ Å^3	AD[b] no. raw data: 35437 no. unique data: 24921	0.81 Å	24.72	0.7 × 0.7 × 0.3	0.049

[a] Four-circle diffractometer equipped with a Syntex LT-1 liquid N_2 cryostat. [b] Ag Rotating anode target coupled to MARResearch 18 cm IP Detector equipped with an Oxford Cryosystems He cryostat. [c] Mo Rotating anode target coupled to MARResearch 18 cm IP Detector equipped with an Oxford Cryosystems He cryostat. [d] Water content is expected to be identical at all temperatures; however, because of temperature-dependent disorder, the number of water molecules in the refined models differed. The differences are an artifact of the model building rather than differences in the actual water content of the crystals.

Deconvoluting disorder in crystal structures is a tenuous process subject to errors in interpretation. Confidence in the results in this study is gained from an examination of the guest−guest steric interactions in the crystals using the electrostatic potential surfaces generated by the theoretical calculations for the isolated guest molecules. Figure 3 presents stereoscopic projections for selected examples from the room-temperature and 20 K structure determinations. The drawings were prepared by superposing the energy minimized structures from the ab initio calculations on the selected guest molecules in the crystal structure and then displaying the calculated electrostatic potentials.

TABLE 2: Final Least-Squares Refinement Statistics

T (K)	no. parameters/ no. restraints	no. reflections ($F_o > 4\sigma F_o$)	$R1$ ($F_o > 4\sigma F_o$)	wR_2 ($F_o > 4\sigma F_o$)	GOF ($F_o > 4\sigma F_o$)	$\delta_\rho$max/$\delta_\rho$min
298	1648/67	10224	0.079	0.235	1.040	0.61/−0.63
270	1677/62	12178	0.089	0.252	1.105	0.62/−0.45
265	1623/3	11104	0.1056	0.274	1.319	0.80/−0.76
260	1599/3	11104	0.093	0.226	1.067	0.88/−0.69
220	1719/16	9189	0.082	0.252	1.040	0.80/−0.62
110	1782/67	12804	0.0741	0.200	1.027	1.02/−0.56
20	1806/3	22304	0.087	0.227	1.037	0.81/−0.66

Deuteron nuclear magnetic resonance (NMR) has been used widely for quantitative investigation of rotational motion in solid inclusion compounds.[14,15] Magic angle spinning (MAS) is more powerful than the older quadrupole echo technique, especially when combined with very high magnetic field to improve spectral resolution. Figure 4 shows the central region of a deuteron MAS spectrum of *N*-acetyl-L-phenylalanine methyl ester (α,*β*,*β*,2,3,4,5,6-d_8) in *β*-cyclodextrin, obtained at 320 K and 17.6 T (115.1 MHz). Well-resolved peaks are observed for the aromatic, CD, and CD_2 deuterons. At this temperature, the line widths (<0.5 ppm) are characteristic of rapid motion and the absence of residual quadrupole splitting implies that this motion is essentially isotropic.

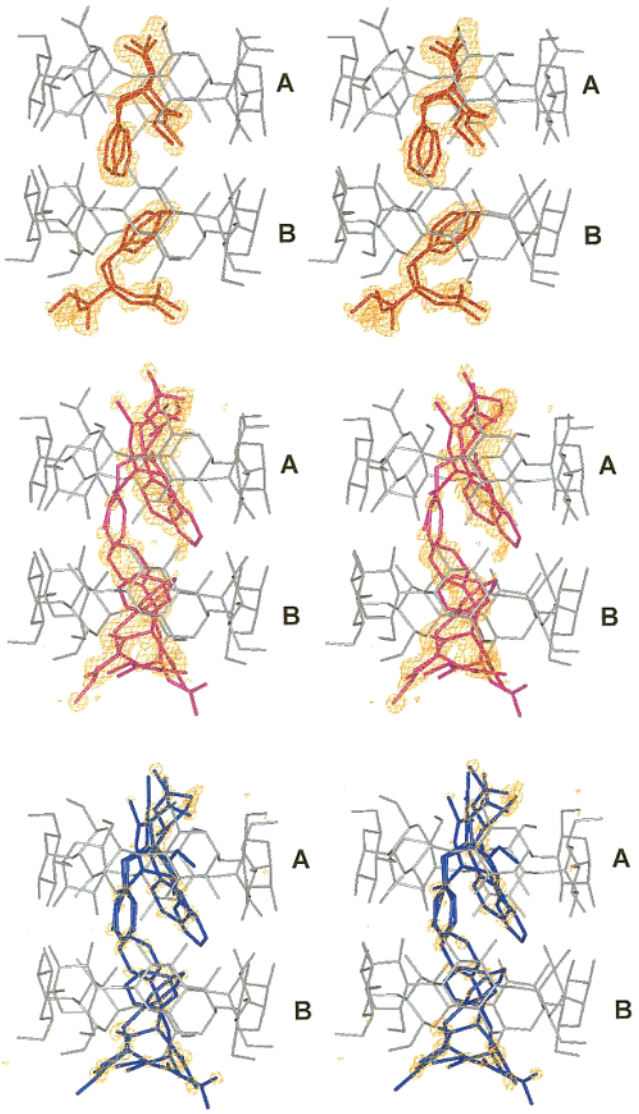

Figure 1. Stereoscopic projection of the difference electron density in the guest region of the 2:2 *β*-CD/*N*-Ac-L-FOMe complex. Contours are plotted at 0.6 $e^-/Å^{-3}$. Disordered guest molecules fit to the electron density at each temperature are illustrated in red (room temperature), magenta (220 K), and blue (20 K). At all temperatures, at least two disordered guests per monomer are shown; only one guest molecule is physically present at any time. The entire CD dimer is shown in gray; waters of hydration are omitted for clarity.

Measurements of temperature-dependent MAS line shapes for air-dried samples of *N*-acetyl-L-phenylalanine methyl ester (α,*β*,*β*,2,3,4,5,6-d_8) in *β*-cyclodextrin are shown in Figure 5. At room temperature (300 K), motional averaging of the quadrupole tensors is not quite complete, and spinning side bands appear at multiples of the spin rate (15 kHz). The intensity profile and width of the spinning side bands can, in principle, be analyzed in terms of specific motional models to yield quantitative information about the rates and trajectories of complex rotational motion.[16] For the case at hand, this procedure is best done by using the results of variable temperature single-crystal X-ray studies to constrain the trajectories. Simulations, based on an electric field gradient tensor that jumps among four orientations pointed at the corners of a tetrahedron, show that the motional rate just below room temperature is on the order of 10^4 jumps/s. However, the simple jump model used in these preliminary simulations predicts very significant loss of overall intensity in the intermediate rate regime ($\sim 10^6$ jumps/s) and this is not observed. A more gentle dependence of overall intensity on motional rate is characteristic of small angle jumps or, better, rotational diffusion.

Even without more detailed analysis, the spectra shown in Figure 5 correlate well with the crystallographic results. As illustrated in Figures 1−3, the crystal structure shows increasing complexity in the packing of guest molecules as the temperature of the crystal is decreased. At 265 K, the crystal structure is very similar to the room-temperature structure, whereas the NMR shows slowed motion of guest molecules at 270 K, very likely arising from the changes defined crystallographically at lower temperatures. At 230 K, the NMR spectrum indicates even further slowing of jumps, which correlates nicely with the crystal structure at 220 K where the changes in crystal packing are clearly observed.

Host Structure. The structure of the host dimer changes little as a function of temperature; only primary hydroxyls experience noticeable conformational change. A superposition diagram for the host molecules at different temperatures demonstrates how minor the changes are; the diagram is included in the Supporting Information. At room temperature, there are two primary hydroxyls, O6(1) and O6(5), that are disordered in either (+) gauche or (−) gauche conformations. A number of other primary hydroxyls show librational disorder indicated by larger atomic displacement parameters. As the temperature is lowered, additional disordered hydroxyl sites are frozen out. At 220 K, primary hydroxyl O6(9) was also modeled with two hydroxyl sites, (+) and (−) gauche; at 20 K, primary hydroxyl O6(7) also exhibits disorder that was modeled with (+) and (−) gauche conformations.

Water Structure. The distribution of water molecules are more strongly influenced by crystal temperature. At room

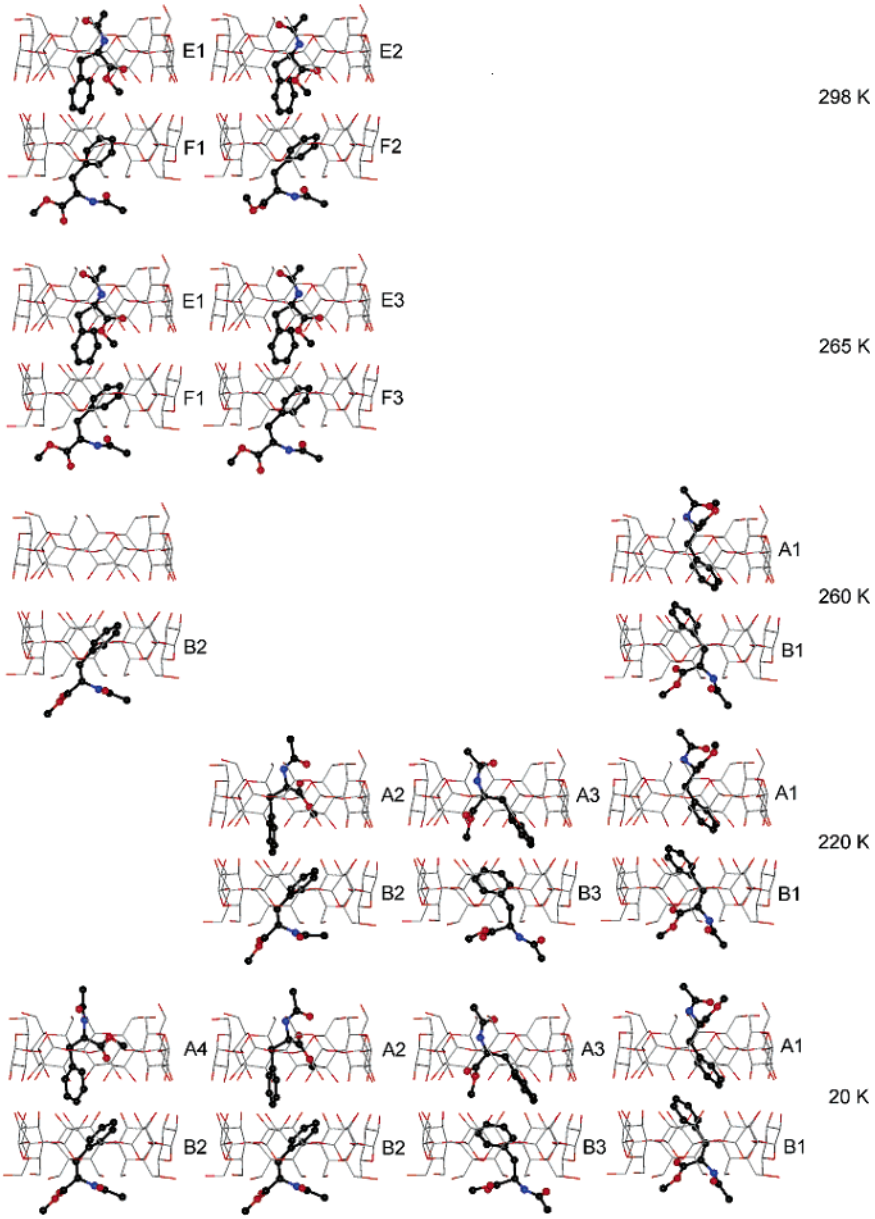

Figure 2. Disorder of the guest molecules has been deconvoluted to illustrate pairs of molecules thought to be present simultaneously in the 2:2 β-CD/*N*-Ac-L-FOMe complexes. All images are drawn with the same orientation of the β-CD molecules to facilitate recognition of the changes in guest molecule conformations, positions, and orientations. The CD dimers are shown in color-by-atom representation, with gray carbons and red oxygens. Guest molecules are also shown in a color-by-atom representation, with black carbons, red oxygens, and blue nitrogen atoms. Hydrogen atoms and waters of hydration are omitted for clarity.

temperature, many water molecules were disordered and were modeled by several split positions. Most of the disordered waters at room temperature are typically frozen into either segregated split positions or a single position at low temperatures. Although in general the locations of waters of hydration are conserved at low temperatures, several water positions change by a small but significant amount; at 20 K some of the water molecules differ in position anywhere from 0.5 to 1.0 Å from their counterpart(s) at room temperature. For example, the general location of water w24 is the same in the 298 and 20 K structures, but the positions in the unit cell differ by ~0.7 Å.

Guest Molecules. The guest molecules were most affected by changes in crystal temperature. Fortunately, the chemical structure of the guest molecules is highly favorable for deconvoluting the crystallographic disorder. The results are discussed first in terms of the observed electron density distribution for the guest molecules and then in terms of their location in the complex and their conformations.

Trends in Guest Electron Density. The distribution of the electron density for the guest regions differs as a function of temperature. At room temperature, the guest electron density has a diffuse, elongated appearance that we believe represents dynamic disorder. At 220 K, the electron density in the guest region is sharpened and peaks are less elongated. The electron density distribution indicates entirely new disordered guest sites. The distribution of the density at 20 K is very similar to that at 220 K, but peaks display nearly spherical rather than ellipsoidal shapes. Disorder present at 220 K appears to indicate static disorder with significant local motion, where a number of guest molecule conformations, positions, or orientations are observed in different domains of the crystal. At 20 K, the local motion appears to be minimal.

Deconvolution of the Disorder: Temperature-Dependent Guest Conformations, Positions, and Orientations. At room temperature, the refined model consists of a 2:2 dimer containing two equally populated disordered guest molecules (E1 and E2

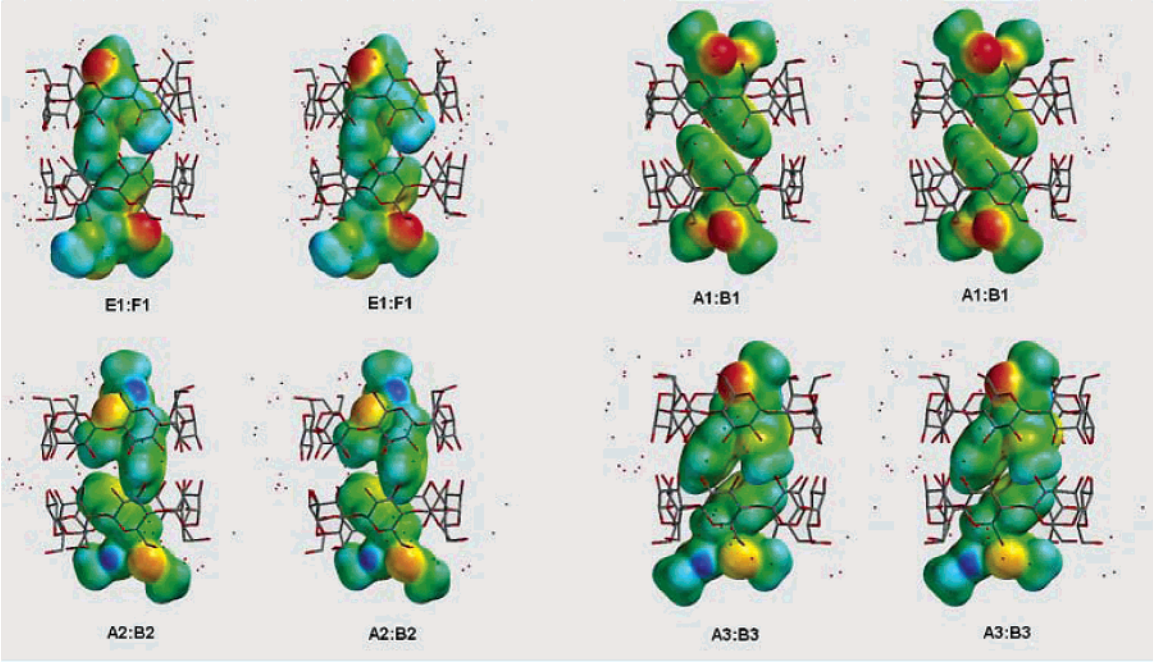

Figure 3. Stereoscopic projections illustrating the steric interactions between gust molecules believed to be present simultaneously in the complex. The guest molecules are presented as electrostatic potential surfaces determined in the ab initio calculations.

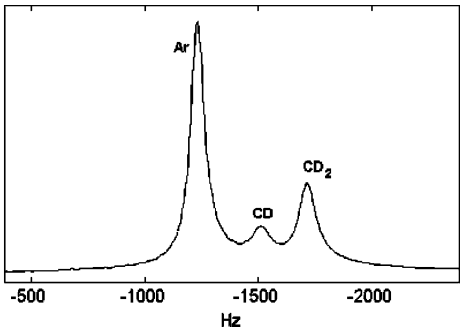

Figure 4. Deuteron MAS spectrum of *N*-acetyl-L-phenylalanine methyl ester (α,*β*,*β*,2,3,4,5,6-d_8) in *β*-cyclodextrin (115.1 MHz, 320 K). The full spectral width is 400 kHz; a 2000 Hz window centered near the carrier frequency is shown. The very narrow Lorentzian lines (<20 Hz) and absence of spinning side bands observed at this temperature are characteristic of rapid, isotropic motion. Peak assignments are based on the observed relative intensities, Ar:CD_2:CD = 5:2:1.

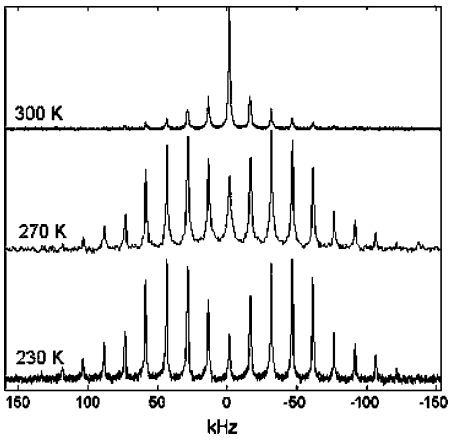

Figure 5. Variable temperature, 115.1 MHz deuteron MAS spectra of *N*-acetyl-L-phenylalanine methyl ester (α,*β*,*β*,2,3,4,5,6-d_8) in *β*-cyclodextrin. At 230 K the side band line widths and intensity profile are characteristic of slow motion (jump rates less than 1×10^4 s^{-1}). The gradual collapse of side bands into a strong center band at higher temperatures implies the gradual onset of isotropic motion.

in Figure 2) in monomer A, and two disordered guest molecules (F1 and F2) in monomer B. In each monomer, the disordered guest conformations are very similar but are slightly displaced from one another. Considering the shape of the electron density at RT, the disorder is believed to be dynamic, with the two positions representing approximate extremes for the thermal motion. The phenylalanine side chains are located inside the hydrophobic interior of the *β*-CD dimer and pack in an edge-to-face arrangement (distances between the phenyl ring midpoints for the two pairs are 4.69 and 4.83 Å). In monomer A, the ester moieties of the guest backbones are positioned inside the torus, whereas in monomer B both the acetyl and ester substituents of the guest backbones protrude outside of the torus, near the hydrophilic primary hydroxyl rim of the CD dimer.

A dramatic change in guest conformations, positions, and orientations take place between 260 and 265 K. All of the guest molecules observed at 298 and 265 K pack in an edge-to-face arrangement, with some evidence for decreased thermal motion as the temperature is decreased. At 260 K a new pair of disordered guests is observed in which the phenyl rings are packed in a parallel arrangement (centroid-to-centroid distance = 3.89 Å). These new guests are in different positions inside the torus, and the guest backbone tails protrude outside of the torus, toward the primary hydroxyl groups; that is, neither guest displays its ester backbone tail extending toward the center of the dimer in the manner observed at higher temperatures. Besides the pair of face-to-face stacked guest molecules, one additional guest site was located in monomer B at this temperature.

At 220 K, three more guest sites were located in electron density maps to give a total of six different deconvoluted guest sites (three sites per monomer). By comparison, electron density maps for the 220 K structure displayed considerably better resolution than those for the 260 K structure. Not surprisingly, the electron density maps for the guest region of the 20 K structure displayed even higher resolution; the density is nearly spherical, as expected for nearly stationary atoms. In the 20 K structure, evidence for one additional guest site was observed at very low levels of electron density (~0.35 $e^-/Å^3$), resulting

TABLE 3: Aromatic Ring Centroid to Glycosidic Oxygen O4 Mean Planes Distances

guest molecule	distance (Å)	difference[a] (Å)
E1 (298 K)	3.26	
E2 (298 K)	3.36	
A1 (20 K)	1.80	1.51
A2 (20 K)	2.81	0.50
A3 (20 K)	2.90	0.41
A4 (20 K)	2.65	0.66
F1 (298 K)	0.64	
F2 (298 K)	0.36	
B1 (20 K)	−2.01	−2.51
B2 (20 K)	−0.38	−0.88
B3 (20 K)	−0.32	−0.82

[a] The difference from the average centroid position for the guest molecules at room temperature. A positive difference indicates a shift away from the center of the extended β-CD dimer (with respect to Figure 6, up for monomer A and down for monomer B).

in a total of seven observable guest sites. A figure presenting the density at this level and a table of occupancy factors for guest molecules are included in the Supporting Information.

The crystallographic models for the structures from 298 to 265 K show that guest molecule conformations, positions, and orientations are very similar. Guests observed at 260, 220, 110, and 20 K are also very similar; however, the latter group differs dramatically form the former one. Consequently, we focus on a comparison of the room temperature and 20 K guest molecules. At low temperatures, the guests with the highest population are the pair of molecules that interact in the hydrophobic torus with face-to-face stacked phenyl rings (A1 and B1). In addition to this pair, five other guest molecules with different conformations, positions, and orientations are observed at 20 K. Guest molecules A2, A4, and B2 adopt room-temperature-like conformations, but are oriented differently with respect to the host dimers, and their backbone functional groups show conformational changes. Guest molecule A3 is observed in a room-temperature-like conformation and position, but with a completely different orientation in the torus. Guest molecule B3, which most likely packs in an edge-to-face arrangement with guest A3, has a new conformation, position, and orientation not observed at room temperature. Figure 3 presents a comparison of the guest molecules at 298 and 20 K.

The phenylalanine side chains for all of the guest molecules are found only in the most hydrophobic environment, which is near the middle of the extended torus of the host dimer. By comparison, the pseudopeptide backbones display greater flexibility in location and conformation. The changes in the guest molecule distributions in the supramolecular complex can be described in terms of two components: location (that is, position and orientation within the host system) and conformation.

Location: Position and Orientation. When the temperature is decreased, a number of changes in guest molecule orientation and position take place. To quantify the changes in position of the disordered guest molecules, mean planes were calculated through the glycosidic oxygen atoms of the respective monomers: ($O4_A$ from O4(1)-O4(7), A monomer; $O4_B$ from O4(8)-O4(14), B monomer), and the distances from the aromatic ring centroid of the respective guests to these mean planes were calculated (Table 3); Figure 6 illustrates the position changes. The most dramatic changes take place for guest molecules in the A monomer. Room-temperature guests E1 and E2 are included most deeply in the extended torus, (respective aromatic ring centroid to $O4_A$ mean plane distances of 3.26 and 3.36 Å). Because we regard the disorder at room temperature to be dynamic, we have chosen the average displacement of these molecules as a reference point for estimating displacement in the guests at low temperature, Table 3. At 20 K guest molecule A1 has shifted upward in the extended torus by 1.5 Å, the aromatic ring centroid now located only 1.80 Å from the mean $O4_A$ plane. For guests A2 and A3, the aromatic ring centroids are shifted 0.50 and 0.41 Å from the dimer center, whereas A4 is shifted in the same direction by 0.66 Å with respect to the room-temperature reference point.

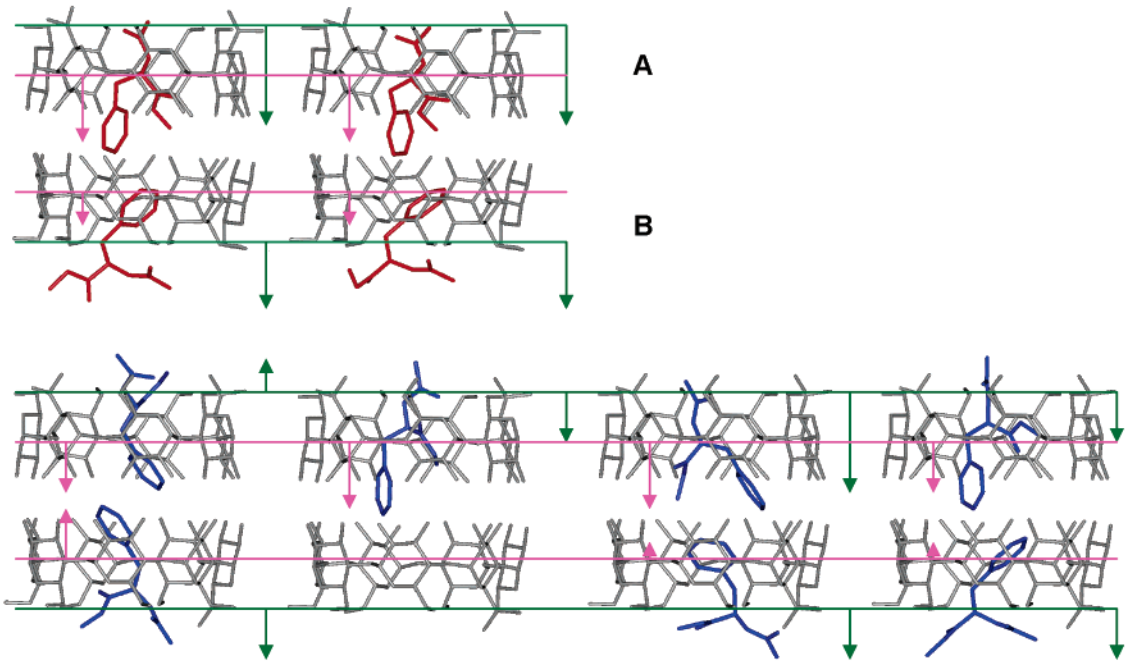

Figure 6. Illustration of the positions of guest molecules in the β-CD dimers. The positions of aromatic ring centroids are illustrated with magenta arrows extending from the mean planes through O4 atoms indicated with magenta lines; distances are listed in Table 3. Backbone locations (Table 4) are illustrated with green arrows, extending from the mean planes through the C6 atoms indicated with green lines. β-CD molecules are shown in gray. The room temperature and 20 K guests are shown in red and blue, respectively.

In the B monomer, some significant shifts are also observed. At room temperature, guest molecules F1 and F2 have aromatic ring centroids located 0.64 and 0.36 Å below the mean $O4_B$ plane. At 20 K guest B1 shows the largest change in position relative to the structure at room temperature; B1 is shifted toward the dimer center by 2.51 Å from the room-temperature reference point. Guest B2 at 20 K bears the most similarity to guests in the B monomer at room temperature. The aromatic ring centroid of B2, however, is shifted by ~0.74 and 1.02 Å from the reference point. Guest molecule B3 shares roughly the same aromatic ring centroid position as room-temperature guest F1, with a difference of only 0.15 Å, although the conformation of B3 is unlike that of guest molecule F1.

Most importantly, in both monomers none of the guest molecule positions observed at 20 K are identical to those at 298 K. Guest molecules, adopting different conformations, are able to dock inside the β-CD dimer and adopt a variety of positions. This flexibility in position implies that the host environment is very nonconstraining, a property that reflects the fact that the guest molecule volume is significantly smaller than the host torus volume. This non-constraining host environment allows the guests to adopt more than one conformation and intermolecular interaction scheme in the binding region presented by the crystal lattice.

The non-constraining host environment also allows the orientations of the guest molecules to change with temperature. For example, at 20 K, dramatically different guest molecule orientations are observed; see Figures 2 and 5. In addition to general differences in molecular orientations and conformations of guest molecules, differences in aromatic interactions between guest molecules in a given dimer are also observed. Only one pair of guest molecules at 20 K has phenyl rings that stack in an antiparallel face-to-face arrangement; several pairs at room temperature and at 20 K display edge-to-face type aromatic packing arrangements.

Backbone Locations. Although the above discussion addresses the magnitude of positional changes for the guest molecules as reflected by the positions of the aromatic rings, no indication of backbone location is obtained. Backbone locations also change significantly with temperature; an analogous calculation was performed, employing a mean plane calculated through the C6 methylene carbon atoms of the D-glucose residues for each monomer ($C6_A$:C6(1)-C6(7), monomer A; and $C6_B$:C6(8)-C6(14), monomer B). Distances from backbone atoms of each guest molecule to the appropriate mean plane were calculated, and an average backbone center position determined for each guest molecule (Table 4). Figure 6 also illustrates the backbone positions for the 298 and 20 K guests. At room temperature, the ester backbones of the guest molecules in A are "included" inside the β-CD torus. The acetyl backbones barely protrude from the primary hydroxyl region. The average backbone distances from the C6 mean plane are 2.54 and 2.76 Å for E1 and E2, giving a reference point 2.65 Å toward the torus center from the $C6_A$ plane. The guest molecule backbones in B protrude from the CD primary hydroxyl region. Average backbone distances from the $C6_B$ mean plane are 2.22 and 1.77 Å for guests F1 and F2 (reference point displaced −1.95 Å toward the hydrophilic interdimer region of the crystal from the $C6_B$ plane). At 20 K, the guest molecules A1 and B1 are face-to-face stacked guests that have changed position and orientation significantly from the comparable guests at room temperature. The guest backbone locations are also different. The average backbone displacement from the A and B monomer reference points are 3.13 Å for A1 and −0.22 Å for B1, indicating that, for this pair, both guest molecules protrude from the respective C6 mean planes toward the hydrophilic interdimer region of the crystal, though the exposure of the B1 backbone is reduced compared with that at room temperature. This backbone exposure is different from that observed for the guests at room temperature, where one guest in A in included to a significant depth in the dimer while the guest in B protrudes almost entirely into the hydrophilic region. Both guests A2 and A4 have room-temperature-like conformations, including the backbone portion of the molecule. However, their average backbone distances from the C6 mean plane are 1.18 and 0.92 Å, which is significantly different (Table 4) from the reference point derived for the room-temperature guest molecules E1 and E2. Guest B2 is also room-temperature-like, with a shift of 1.50 Å from the $C6_B$ mean plane. This distance from the respective reference point is −0.50 Å, indicating reduced exposure of the backbone to the hydrophilic interdimer region. Guest molecule A3 has both a conformation and position similar to those observed for E1 and E2, but a different orientation. The backbone penetration depth of A3 is very close to the reference point for the A monomer at room temperature, Table 4. Guest molecule B3's average backbone position is located 1.39 Å from the $C6_B$ mean plane. In summary, at 20 K the B monomer guests penetrate to similar depths in the torus, whereas the A monomer guests show more variability in backbone penetration in the torus.

TABLE 4: Backbone Locations: Average Backbone Distance from Methylene Carbon Atom (C6 of D-Glucose Residues) Mean Planes

guest molecule	average backbone atom distance (Å)	difference[a] (Å)
E1 (298 K)	2.54	
E2 (298 K)	2.76	
A1 (20 K)	−0.48	3.13
A2 (20 K)	1.18	1.47
A3 (20 K)	2.61	0.04
A4 (20 K)	0.92	1.73
F1 (298 K)	2.22	
F2 (298 K)	1.77	
B1 (20 K)	1.31	−0.22
B2 (20 K)	1.50	−0.50
B3 (20 K)	1.39	−0.60

[a] The difference from the average backbone atom position for the guest molecules at room temperature. A positive difference indicates a shift away from the center of the extended β-CD dimer, that is, toward the hydrophilic interface (with respect to Figure 64, up for monomer A and down for monomer B).

Conformational Differences. In addition to observing significant changes in position and orientation of the disordered guest molecules, significant conformational changes are also observed. Torsion angles describing the molecular conformations of the different guest molecules at 298 and 20 K are listed in Table 5. These interactions are illustrated in Figures 3 and 7, which display the theoretically calculated molecular dipoles for the guest molecules. Figure 7 was prepared to facilitate comparison of the respective orientations of the dipoles (the bottom molecule in each complex are in similar orientations) and provide an illustration of the conformational differences in the depsipeptide backbones.

Guest molecules at room temperature display the most modest conformational changes with the difference confined to the ester moiety of the backbone. Although the change in conformation is modest, it has a dramatic effect on the orientation of the molecular dipole. Guest molecules B1 and B3 also display relatively modest changes in backbone conformation; once again the orientations of the molecular dipoles are significantly

TABLE 5: Torsion Angles Describing Conformations of the Disordered Guest Molecules

guest	ω	φ	ψ	χ_1	χ_2
A1	176.64	−100.46	69.50	−176.10	79.43
A2	178.04	−86.73	151.36	173.59	−102.35
A3	176.40	−146.23	136.93	−179.62	150.21
A4	−179.39	−114.99	−23.90	−139.23	−83.29
E1	−177.82	−167.86	174.88	98.66	118.19
E2	176.59	−162.50	174.81	84.24	106.74
B1	167.06	−95.02	71.28	−165.88	68.17
B2	−176.85	−112.65	103.42	−61.08	116.95
B3	170.82	−127.03	134.28	179.98	88.38
F1	−179.38	−124.26	174.80	−57.60	90.20
F2	175.54	−135.79	118.41	−45.10	96.23
NG[a]	176.93	−81.00	155.91	−76.22	91.64

[a] Neat guest molecule (structural details reported in ref 8).

different. In contrast, molecule B2 displays a very different backbone orientation (note χ_1 torsion angles in Table 5). At 20 K, the molecules of the most highly populated guest pair (A1 and B1) are new conformers. A1 differs from conformers E1 and E2, with different conformations observed for both the backbone and side chain. Guests (20 K) A2 and A4 have more similar phenyl ring conformations compared to the room-temperature guests but differ in conformations of the ester and acetyl backbone moieties. Guest A3 has a conformation very similar to the room-temperature guests, but the orientation of the entire guest molecule is different. The 20 K guest B1 has a totally different side chain conformation from that observed at room temperature, and changes are also observed in the ester backbone conformation. The 20 K guest molecule B2 has a conformation very similar to those observed for guests F1 and F2 at room temperature, with slight torsional differences observed for the ester backbone.

For guest molecule B3, noticeable conformational differences are observed when compared to both the room-temperature B guests and the other 20 K B guests.

In Figure 8, the guest molecules from the 298 K (red) and 20 K (blue) structures are shown with the acetyl backbone atoms superimposed. The acetyl portion of the molecules changes little, adopting the expected trans peptide bond conformation. Guests from the A monomer are shown in the top diagram; the guests in the B monomer are shown in the bottom monomer. Along with those guest molecules, the molecular conformation observed in the neat crystal structure of *N*-Ac-L-FOMe is shown in a color by atom scheme.[17] This picture provides a more visual comparison of the variability in conformations observed from 298 to 20 K. It is immediately apparent that room temperature and 20 K guests have significant differences in conformations; none of the room-temperature guests have a conformation identical to any conformation observed at 20 K. Also interesting is the observation that none of the guest molecules observed in the complex at any temperature have the conformation observed in the neat crystal structure. Relative energies from the ab initio calculations for the conformations observed in the crystal structures are presented in Table 6. With the exceptions of molecules F2 and A4, the conformational energies fall within a narrow range. Molecule F2 appears to contain some conformational strain in the depsipeptide backbone. Molecule A4 has more conformational strain than the other examples in the crystal at 20 K; it should be noted that A4 has the lowest population parameter of any guest molecule characterized. The differences

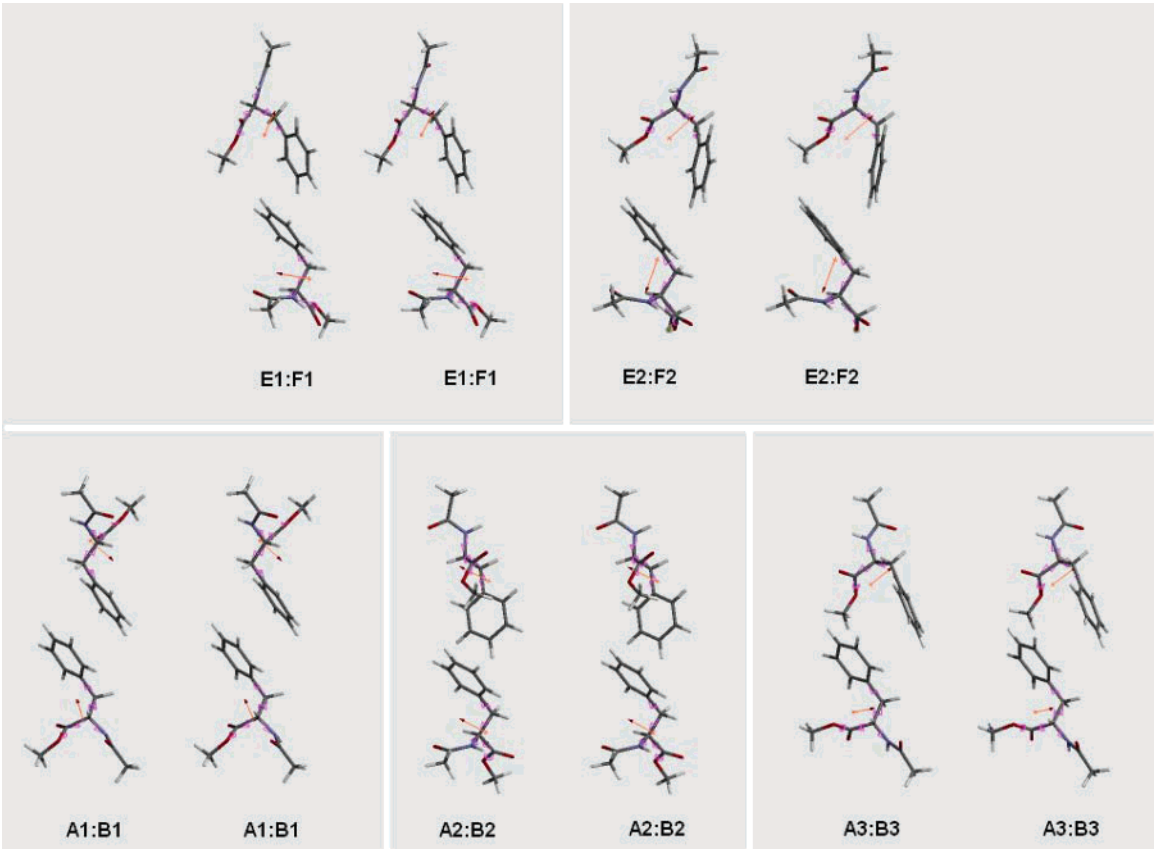

Figure 7. Stereoscopic projections illustrating the relative orientations of guest molecule dipoles from the ab initio calculations. The bottom molecules in each pair have been similarly oriented to facilitate visual comparison. The figure also illustrates the differences in backbone conformations of the guest molecules and the differences in the respective orientations of the phenyl rings in each complex.

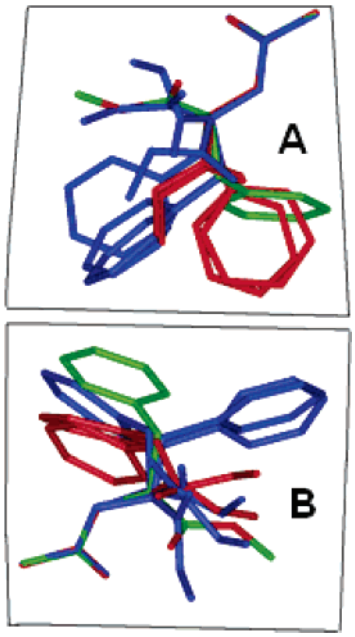

Figure 8. Superposition diagram illustrating differences in conformation of the guest molecules. The pseudopeptide bond was used as the common structural moiety in preparation of the diagram. The guest molecules shown in red are those from the 298 K structure; guests shown in blue are those from the 20 K structure. The molecule colored-by-atom type with green carbon atoms, red oxygen atoms, and blue nitrogen atoms is the molecular conformation observed in the neat crystal structure.

TABLE 6: Relative Energies for the Molecular Conformations Observed in the Crystal Structures Resulting from the ab Initio Calculations

molecule	rel. E (kcal/mol)	molecule	rel. E (kcal/mol)	molecule	rel. E (kcal/mol)
E1[a]	0.00	A1[b]	1.09	B1[b]	1.44
E2[a]	−2.06	A2[b]	1.77	B2[b]	0.55
F1[a]	−1.28	A3[b]	1.18	B3[b]	−1.43
F2[a]	11.15	A4[b]	4.95	neat crystal[b]	−0.18

[a] Starting model derived from the crystal structure at 298 K. [b] Starting model derived from the crystal structure at 20 K. [c] Starting model derived from the crystal structure at 298 K in the neat *N*-Ac-L-FOMe crystal structure.

in conformational energy are easily compensated for by hydrogen-bonding energy contributions to the complex as a whole.

Hydrophilic Interactions in the Interdimer Region of the Crystal. The observation of different guest positions, orientations, and backbone conformations from 298 to 20 K reflects not only a high degree of molecular flexibility inside the nonconstraining torus of the extended dimer but also significant variations in intermolecular interactions. Hydrogen bonding involving *N*-Ac-L-FOMe molecules takes place in the hydrophilic crystal space between the dimeric hosts. In this region, primary hydroxyls of neighboring CDs and waters of hydration are available for interaction. Because it is easier to compare interactions observed in one particular monomer, hydrogen-bonding interactions observed in A will be discussed first (Figure 9), followed by the B guest hydrogen-bonding interactions (Figure 10). Distances for the hydrogen-bonding interactions (illustrated in Figures 9 and 10) are listed in Tables H1 and H2 (supplementary material). Hydrogen-bonding interactions in A involve a framework of primary hydroxyls: O6(1a), O6(8), O6(9), O6(11), O6(12), and O6(14) and six water of hydration molecules: w17, w18, w19, w31, w33, and w40. Some defining interactions in the A binding region are invariant, regardless of the disordered guest molecule present. Primary hydroxyls O6(8) and O6(12) from another dimer interact directly, whereas the remaining primary hydroxyls interact with one another via waters of hydration. Primary hydroxyl O6(11) interacts via water w17 with O6(8), and interacts via bridging waters w17 and w33 with O6(9).

Both primary hydroxyls O6(1a) and O6(14) interact with water w19, which is an important water in the guest hydrogen-bonding scheme.

At 298 K, both of the two disordered guest molecules (E1 and E2) have ester backbone moieties included inside the β-CD torus, a location where they are unavailable for interactions to take place with waters of hydration or primary hydroxyls in the hydrophilic interdimer region. The acetylated backbone moieties are located near the primary hydroxyl rim of the dimer; close enough to interact with water w31. Water w31 then interacts with water w19 and primary hydroxyl O6(8). Water w19 is well-ordered, anchored by interactions with O6(1a) and O6(14) as mentioned above and an additional interaction with water w18.

At 20 K, the same basic framework of waters of hydration molecules and primary hydroxyl groups undergo hydrogen-bond interactions. The guest molecule A1 at 20 K has a very different conformation, position, and orientation from the room-temperature guests E1/E2. Both backbone moieties are located near the hydrophilic interdimer region. The ester oxygen is involved in a rather long hydrogen-bonding interaction with primary hydroxyl 5a. The acetyl oxygen no longer interacts with w31, instead the amide nitrogen serves as a hydrogen bond donor to w31. Note that in changing temperature the donor−acceptor properties of w31 changed, illustrating the flexible nature of intermolecular interactions in this system.

Both guests A2 and A4 are molecules that are room-temperature-like, however, the hydrogen-bond interactions are different. For A2, the amide nitrogen interacts with w31, rather than the acetyl oxygen. Again, water w31 has undergone donor−acceptor switching when compared with the room-temperature interactions. The ester moiety has a slightly different conformation than in E1/E2. The carbonyl oxygen of the ester backbone interacts with water 40. Guest molecule A4 is present only 10% of the time in the complex; the acetyl backbone was not located well. The ester moiety was observed; the ester oxygen interacts with w40. Interactions with w31 are not possible because the water w31 and guest A4 cannot be present simultaneously.

Hydrogen-bonding interactions in the B monomer are more complex. Interactions take place between the guest molecules and disordered waters of hydration and a few different primary hydroxyls, one of which is also disordered. Primary hydroxyls O6(2), O6(6), O6(3), and O6(5a/b) define the framework for this binding region. Water molecules involved in hydrogen-bond interactions with the primary hydroxyls and guest molecules are w24, w26, w29, w30, and w39. The binding region for guests in the B monomer has a few invariant interactions, regardless of the disordered guest molecule present. Primary hydroxyls O6(2) and O6(6) (from a neighboring dimer) interact directly with one another, O6(6) also interacting with water w16. Primary hydroxyl O6(3) interacts with water w30, which also interacts with nearby water w29.

The room-temperature guest molecules F1 and F2 experience hydrogen-bond interactions via the amide nitrogen and acetyl oxygen atoms. Guest molecule F1 is located close enough to interact directly with neighboring primary hydroxyl O6(5a),

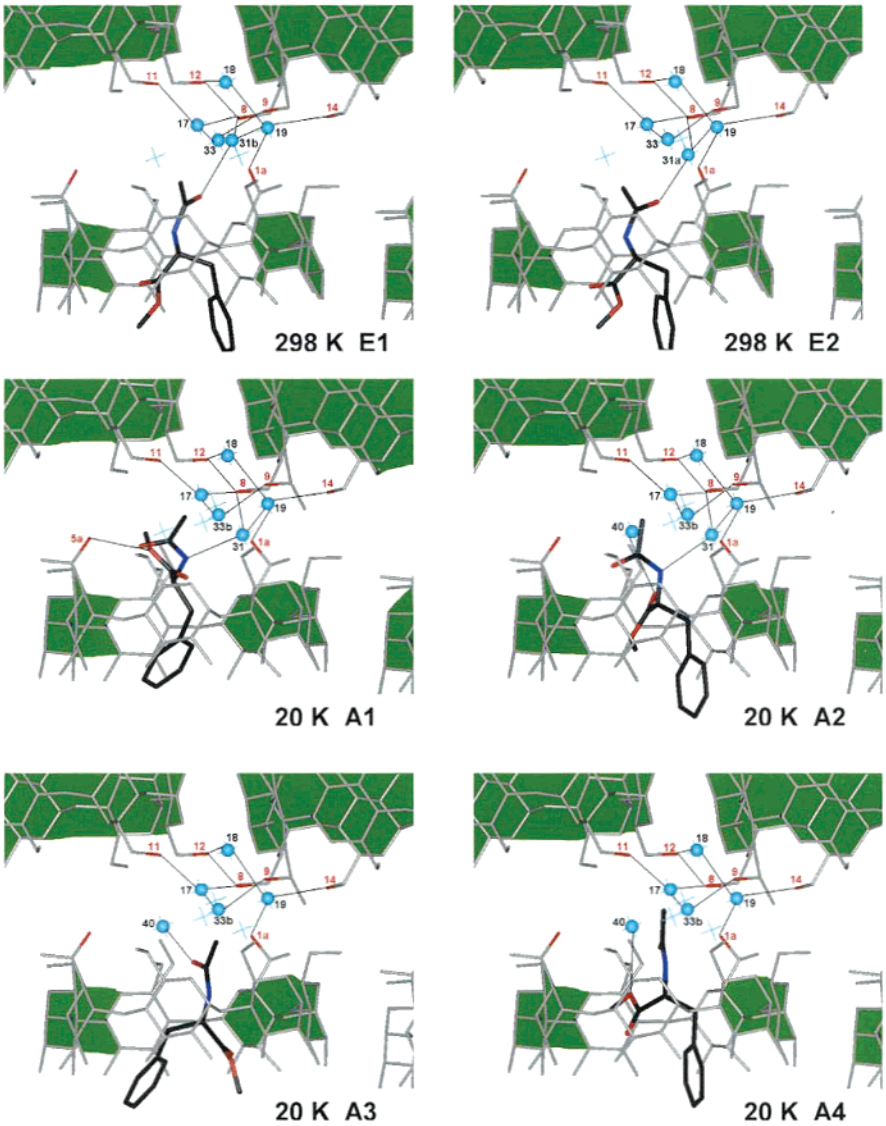

Figure 9. Diagrams illustrating the hydrogen-bonding interactions for different guest molecules in the A monomer. CDs are shown in gray. Only the primary hydroxyls involved in interactions are colored red. Guest molecules are shown in color-by-atom representation with black carbons, red oxygens, and blue nitrogens. Waters of hydration are colored cyan. Green shading helps define the binding region.

whereas F2 interacts with primary hydroxyl O5(5b) via waters w39 and w26. Water 26 also interacts with the well-ordered water of hydration molecules w24 and water 29. The ester oxygen of guest F1 is located close enough to interact with primary hydroxyl O6(5a). For both guests, the acetyl oxygen atoms interact with primary hydroxyl O6(3) from an adjacent dimer.

The 20 K guest molecules B1 and B2 have interactions similar to those observed for guest F2 at room temperature. Both guests have amide nitrogen atoms that interact via waters w39 and w26 with primary hydroxyl O6(5a). For both guests, the acetyl oxygen atoms interact with primary hydroxyl O6(3) from an adjacent dimer, in the same manner as the room-temperature molecules F1 and F2. Although guest molecule B1 has a very different conformation and position in the CD torus compared to the room-temperature guest molecules, the backbone region nonetheless interacts with the same basic set of waters. Guest molecule B2 is more similar to room-temperature guests F1 and F2. The molecular conformation is similar, except for that of the ester moiety, which is reoriented about the α-carbon to carbonyl carbon bond. The overall position of B2 (as characterized by the phenyl ring centroid) in the torus has shifted by ~0.9 and 0.6 Å from the positions of guests F1 and F2 at room temperature. In changing the temperature from 298 to 20 K, the overall positions of waters w39 and w26 have also shifted in the same manner, by about 0.8 Å and 0.5 Å, respectively. Water w26 is still in a location favorable for interaction with the well-ordered water w24 and water 29. Water w24 also shifted at lower temperatures. For guest molecules B1 and B2, guest molecule backbone conformations and water positions in the hydrophilic region of the crystal appear to adapt in order to preserve hydrogen-bonding interactions.

Guest molecule B3 at 20 K has a very different conformation and orientation from the guests observed at 298 K and guests B1 and B2. The position of the phenyl side chain of guest B3 is similar, though, to the position of the phenyl side chain of guest B2. Interactions involving guest B3 are similar in nature to those observed for guests B1 and B2, but involve some different donors/acceptors. Because of conformation changes, guest B3 has an acetyl backbone located closer to primary hydroxyl O6(3). The acetyl oxygen interacts with this primary hydroxyl rather than with O6(2). The amide nitrogen is located too close to water w39 to be physically present at the same

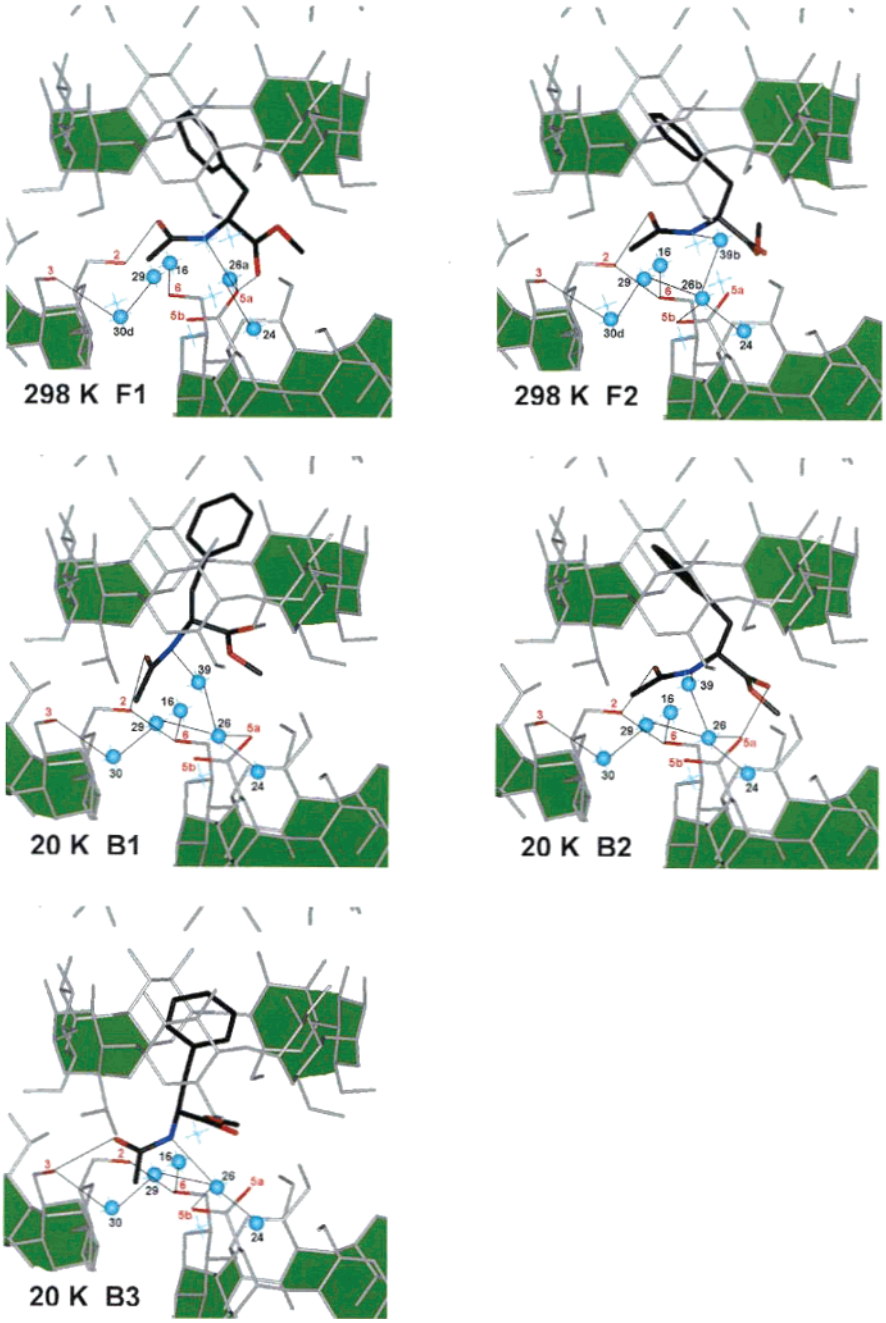

Figure 10. Diagrams illustrating the hydrogen-bonding interactions for different guest molecules in the B monomer. CDs are shown in gray. Only the primary hydroxyls involved in interactions are colored red. Guest molecules are shown in color-by-atom representation with black carbons, red oxygens, and blue nitrogens. Waters of hydration are colored cyan. Green shading helps define the binding region.

time. Instead, the amide nitrogen interacts via water w26 with primary hydroxyl O6(5b).

In summary, guest molecules find several ways to arrange themselves in a nearly constant lattice environment, interacting with available waters of hydration and primary hydroxyls. For each binding region, an invariant scheme of hydrogen bonding is observed between primary hydroxyls and waters of hydration. This scheme defines the binding environment for guest molecules. A small number of waters of hydration change positions in "reaction" to the changes in temperature. Guest molecule conformations, positions, and orientations inside the nonconstraining β-CD torus change with temperature, but guest molecules still dock with the β-CD molecules in the crystal in a manner that achieves interaction with the same or other nearby water of hydration molecules and primary hydroxyl groups. Very similar types of interactions are observed for the guest molecules, even when different donors or acceptors are utilized; most of the differences arise due to changes in position, which also cause changes in the availability of certain groups for interaction. Backbones of the guest molecules adapt to changes that take place in the hydrophobic torus. Host primary hydroxyls do not react, in terms of conformational changes, specifically to changes in guest molecules.

Thermodynamic Considerations. Given that the changes in conformations, positions, and orientations of guest molecules in these supramolecular complexes reflect changes in ΔG as the temperature changes, we hope to gain some insight into the components of ΔS and ΔH that govern the system. At this point, a qualitative description is the best we can do. The electron density plots in Figure 1 provide one indication of changes in

the entropic component as a function of temperature. The degree of sharpening of the difference electron density plotted at constant contour levels as the temperature of the crystal is lowered from 298 to 20 K provides a graphical indication of significantly reduced thermal motion in the crystal at reduced temperature. Furthermore, temperature-dependent changes in electron density for the guest molecules indicate a gradual change from dynamic disorder to static disorder. In terms of enthalpic contributions, there appear to be a number of guest conformations, positions, and orientations with favorable hydrogen-bonding interactions. At 20 K, the observation of several possible disordered guest molecules indicates that many of the disordered guests might have very similar free energies.

Conclusions

A complex pattern of changes in hydrogen-bonding interactions is observed as the crystal is cooled from 298 K to 20K. Changes in guest molecule conformations, positions, and orientations give rise to this phenomenon. Guest molecules are allowed significant degrees of freedom inside the nonconstraining extended β-CD dimer torus, and a number of possibilities for intermolecular interactions with water of hydration molecules and nearby host hydroxyl groups are observed for the different disordered guest molecules. Hydrophilic interactions involving guest atoms adapt to changes in interactions inside the hydrophobic region of the CD.

The results of this temperature-dependent study show that molecular recognition is energy-dependent, especially in weakly constrained environments such as those often found in supramolecular host−guest inclusion complexes. This study provides evidence for the important role that kinetic energy plays in recognition phenomena. We suggest that this particular complex presents a useful model for examining molecular recognition in situations where substrate molecules are docked with a scaffold presenting hydrogen-bonding sites of limited spatial variation. Flexibility in substrate-binding pocket interactions arises from the presence of water molecules that can adapt to provide hydrogen-bonding interactions between the substrate and the binding target.

Also, our results indicate that a thorough examination of host−guest inclusion complex structures should include temperature-dependent studies; additional information not found in a simple room-temperature structure can be obtained. For example, the observation of an apparent transition from a dynamically to statically disordered system as the temperature is lowered provides indications of the importance of kinetic energy in characterizing the model on a classical or quantum mechanical basis. It is hoped that temperature-dependent studies on related systems will provide sufficient structural data to characterize the quantum mechanical model more quantitatively.

The ab initio calculations performed to date have been confined to isolated guest molecules. They have made a valuable contribution to establishing confidence in the deconvolution of the crystallographic disorder and to gaining some insight into the differences in conformational energy of the guest molecules and to characterizing the dipolar interactions of guest molecules in the complexes. Future plans include calculations on a more complex system, most likely using semiempirical methods to obtain some insight into the intermolecular energetics of the system. Said calculations will have to take into account the complexities of disorder in guest molecules and in water molecules. One of the challenges will be to achieve a model for the hydrogen-bonding interactions of water molecules for which data on hydrogen atom positions is not available.

Acknowledgment. This work was supported in part by NSF grants (CHE-9812146 to J.J.S., and CHE0079136 to G.L.H. and R.L.V.). We thank Charles R. Ross, II and Tom J. Brett for technical assistance in data collection and processing.

Supporting Information Available: CIF data for the crystal structure at 298, 270, 265, 260, 220, 110, and 20 K, a tables of guest occupancy factors and selected hydrogen bonding distances, an electron density plot for the A monomer plotted at a lower contour to demonstrate the presence of the two phenyl ring atoms not observed in Figure 1, and a superposition plot of the cyclodextrin dimers of the refined structures at the seven temperatures. This material is available free of charge via the Internet at http://pubs.acs.org.

References and Notes

(1) Gellman, S. H. *Chem. Rev.* **1997**, *97*, 231−232.
(2) Lehn, J. M. *Agnew. Chem., Int. Ed. Engl.* **1988**, *27*, 89−112.
(3) Williams, R. J. P. *Biochem. Soc. Trans.* **1988**, *16*, 923−925.
(4) Cram, D. J. *Science* **1988**, *240*, 760−767.
(5) Schneider, H. *Agnew. Chem., Int. Ed. Engl.* **1991**, *30*, 1417−1436.
(6) Clark, J.; Stezowski, J. J. *J. Am. Chem. Soc.* **2001**, *123*, 9880−9888.
(7) Clark, J.; Booth, B.; Stezowski, J. J. *J. Am. Chem. Soc.* **2001**, *123*, 9889−9895.
(8) Stezowski, J. J. in *Transactions of the American Crystallographic Association*; Stezowski, J. J., Ed., 1985; Vol. 24, p 73−82.
(9) Stezowski, J. J.; Jogun, K. H.; Eckle, E.; Bartels, K. *Nature* **1978**, *274*, 617−618.
(10) Jogun, K. H.; Stezowski, J. J. *Nature* **1979**, *278*, 667−668.
(11) Molecular Simulations, Inc. *InsightII*, Version 980; Molecular Simulations, Inc.: San Diego, CA, 1999.
(12) Nardelli, M. *Comput. Chem.* **1983**, *7*, 95−98.
(13) Mentzafos, D.; Mavridis, M.; LeBas, G.; Tsoucaris, G. *Acta Crystallogr., Sect. B* **1991**, *47*, 746−757.
(14) Hoatson, G. L.; Vold, R. L. *NMR: Basic Princ. Prog.* **1994**, *32*, 1−61.
(15) Ripmeester, J. A.; Ratcliffe, C. I. *Solid State NMR Spectroscopy*; Pergammon Press: New York, 1995.
(16) Huang, Y.; Vold, R. L.; Hoatson, G. L. *J. Chem. Phys.* **2005**, *124*, 104504.
(17) Clark, J. L.; Ross, C.R., II; Stezowski, J. J., to be submitted for publication.